JOURNAL OF GEOPHYSICAL RESEARCH, VOL. 91, NO. C8, PAGES 9709–9719, AUGUST 15, 1986

Simultaneous Spatial and Temporal Measurements of the Internal Wave Field During MATE

MURRAY D. LEVINE

College of Oceanography, Oregon State University, Corvallis

JAMES D. IRISH

University of New Hampshire, Durham

TERRY E. EWART AND STEPHEN A. REYNOLDS

Applied Physics Laboratory, University of Washington, Seattle

A statistical description of the deep ocean internal wave field is presented using measurements from the Midocean Acoustic Transmission Experiment, conducted near Cobb Seamount in the NE Pacific (46°46'N, 130°47'W) during June–July 1977. The unique feature of this experiment is the variety of data obtained simultaneously from the same location: time series of temperature and velocity, and vertical and horizontal profiles of temperature. A generalized form of the Garrett-Munk (GM) internal wave spectrum is developed and used to interpret the data. This spectral model is specified by three parameters, $\tilde{E}$, t, and p (energy level, wave number bandwidth, and frequency spectral slope, respectively). The variety of measurement types permit these three model parameters to be estimated from more than one measurement. The overall best fit values to the MATE data were $p = 2.7$ (GM use $p = 3$), $t = 3.1$ m^{-1} s (equivalent to $j_* = 6$, twice the GM value), and $\tilde{E} = 8 \times 10^{-4}$ J/kg (within 20% of the GM level). Although significant differences were found in the values of the bandwidth (t) and spectral slope (p) from those specified by Garrett-Munk, the deviations are consistent with the behavior expected in a random internal wave field.

1. INTRODUCTION

Our knowledge of internal gravity waves in the ocean has increased dramatically in the past few decades. While internal waves have been observed since the beginning of the century, the pervasiveness of the phenomena has only been realized with the advent of instruments capable of measuring time series of velocity and temperature. However, internal waves are sufficiently complicated that relating observations to theoretical ideas is difficult. In order to resolve the internal wave field, in even a rudimentary way, simultaneous measurements of the vertical, horizontal, and temporal variability of the ocean are necessary. For more background, see recent reviews by *Munk* [1981], *Levine* [1983], and *Olbers* [1983].

The extensive set of environmental and acoustic data gathered during the Midocean Acoustic Transmission Experiment (MATE) provides an opportunity to study simultaneous observations from several different types of measurements. The experiment was conducted near Cobb Seamount in the NE Pacific about 450 km from the coast of Washington (46°46'N, 130°47'W) during June–July 1977 [*Ewart et al.*, 1977]. To accommodate the requirements of the acoustic experiment, the internal wave measurements were made between Cobb Seamount and a second smaller seamount to the southwest in a water depth of 2200 m (Figure 1). Cobb Seamount is an imposing topographic feature rising to within 30 m of the surface; the top of the smaller seamount (labeled "Corn" in Figure 1) is nearly 1000 m below the surface. While the proximity of these two features (about 9 km away) may affect the internal wave field, other studies suggest that the perturbation of the internal wave field is limited to regions very near the seamounts [*Wunsch*, 1976; *Wunsch and Webb*, 1979; *Eriksen*, 1982]. The seamounts, however, could be a significant source of internal tide [e.g., *Baines*, 1982].

The purpose of this paper is to present the variety of temperature and velocity data gathered during MATE and to describe statistically the internal wave field suggested by these observations. The empirical model of *Garrett and Munk* [1972, 1975; hereafter referred to as GM] is used as a framework for comparing the various statistical quantities that could be estimated from the measurements. Guided by the observations, the form of the GM internal wave spectrum is generalized to accommodate an arbitrary frequency spectral slope; this formalism may also be useful in interpreting other observations where the frequency spectral slope differs from the GM model. The unique feature of the MATE observations is that the different types of measurements were made nearly simultaneously in the same part of the ocean. This invites a close comparison with theory, since model parameterizations can be checked for consistency with the same parameters estimated from more than one measurement.

This paper serves as an overview of the data gathered during MATE; the association with internal waves is made by using the GM model as the standardized "yardstick." More detailed analyses and modeling of specific aspects of the data set, such as fine structure [*Levine and Irish*, 1981] and the internal tide, are deferred to other studies.

The observed temperature and velocity measurements and associated spectral quantities are presented in section 2. The observations are compared with internal wave consistency relations in section 3. A generalized form of the GM spectral model is presented in section 3, and the parameters of the model are determined in section 4. A comparison with histori-

Paper number 6C0272.
0148-0227/86/006C-0272$05.00

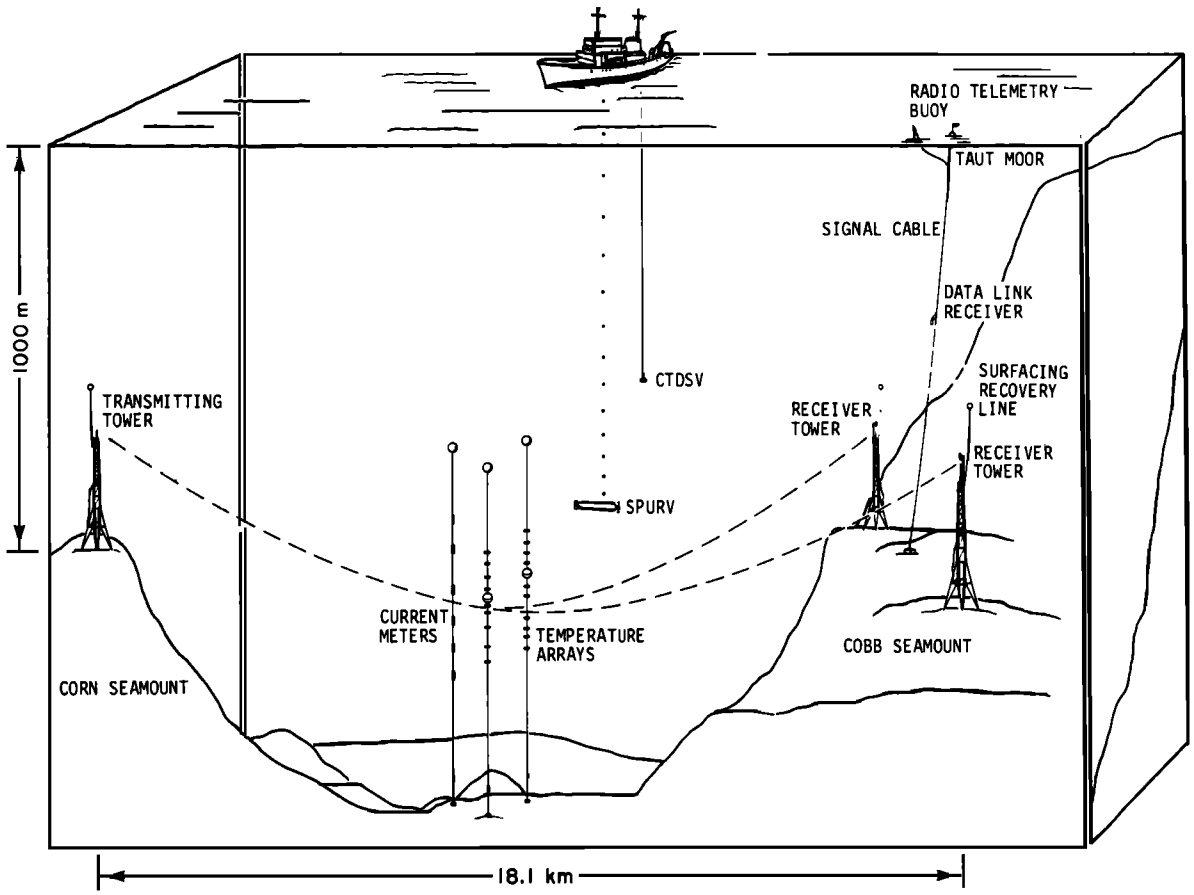

Fig. 1. A schematic overview of MATE showing the three moored arrays, SPURV, CTDSV, and the relationship to the acoustic experiment.

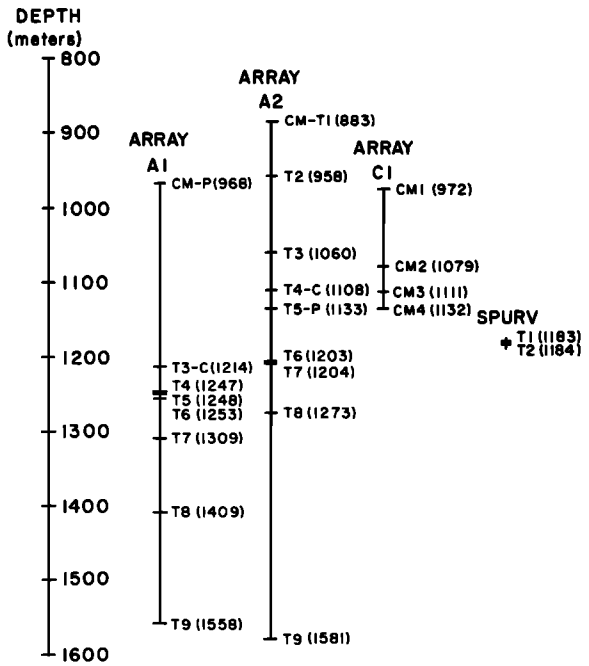

Fig. 2. Depths of the current meters (CM), temperature (T), conductivity (C), and pressure (P) sensors located on arrays A1, A2, and C1 and SPURV.

cal data is made in section 5, and a summary and conclusions are given in section 6.

Throughout the paper units of radians per second (s^{-1}) and radians per meter (m^{-1}) are used exclusively in equations. Units of cycles per hour (cph) and cycles per meter (cpm) are also used in discussions and in presentation of the data.

2. Observations

A schematic overview of the components of MATE is shown in Figure 1. The vertical structure was sampled repeatedly using a conductivity, temperature, depth, sound velocity measuring instrument (CTDSV). Temporal variability at fixed points was monitored with three moored arrays. Two moored temperature arrays (referred to as A1 and A2) and one current meter array (C1) were deployed midway between the two seamounts in 2.2 km of water. Horizontal temperature profiles were obtained with the free-swimming self-propelled underwater research vehicle (SPURV) [*Widditsch*, 1973]. The depths of the moored sensors and SPURV observations are shown in Figure 2.

CTDSV Profiles

A total of 38 CTDSV profiles from the surface to 1500 m were taken at three stations with a Bissett-Berman 9040-5 CTDSV. The primary station was midway between the sea-

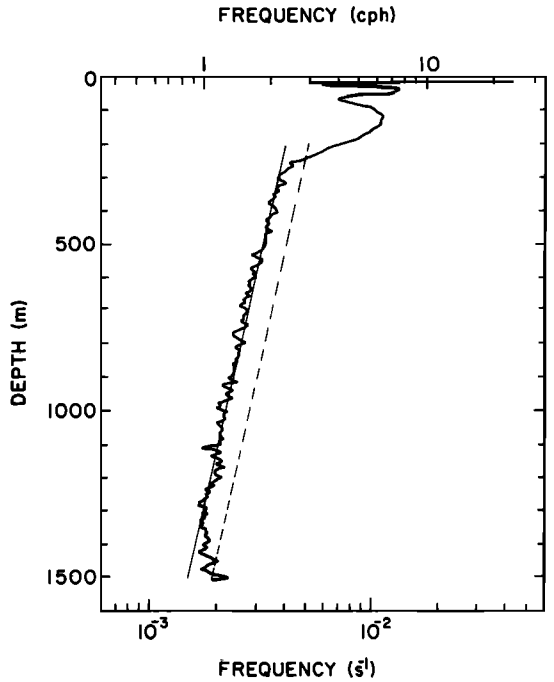

Fig. 3. The average buoyancy frequency profile $N(z)$. The data are fit with an exponential $N(z) = N_0 \exp[-(z - 200)/1300]$ with $N_0 = 4.0 \times 10^{-3}$ s^{-1} (solid line). The average oceanic profile used by *Garrett and Munk* [1972] with $N_0 = 5.2 \times 10^{-3}$ s^{-1} is shown for comparison (dashed line).

mounts near the moored arrays. The other two stations were midway between this central site and each seamount. In addition, at the primary site a 25-hour series of CTDSV profiles was recorded, consisting of a profile from 1000 to 1300 m every 20 min. As the vertical sampling was nonuniform, the profiles were filtered to 1-m intervals with a 2-m triangular filter centered around each 1-m interval. The 38 deep profiles were ensemble averaged to produce profiles representative of the average conditions during the experiment. Since the profiles were taken at somewhat random times, it was assumed that the variations due to tides, internal waves, and nonpersistent structure were nearly averaged out.

The average profiles of temperature, salinity, density, and sound velocity are nearly linear over the depth range of the moored sensors [*Ewart et al.*, 1977]. The buoyancy frequency was calculated from the average profile (Figure 3). Below 200 m the profile is fit to an exponential, as suggested by *Garrett and Munk* [1972], producing a representative profile for determining the local buoyancy frequency, $N(z)$. This profile is consistent with earlier measurements at Cobb Seamount [*Ewart*, 1976].

Vertical wave number temperature spectra were calculated from perturbation profiles formed by subtracting the average temperature profile from each of the 32 profiles made concurrently with the A2 measurements. Each profile was divided into nine depth ranges and Fourier transformed; spectra were estimated by a combination of ensemble and band averaging. Corrections were also made for sensor response. If the temperature fluctuations were caused primarily by the vertical advection of a linear temperature gradient, then the vertical displacement spectra (dropped spectra, DS_ζ), shown in Figure 4, can be formed by dividing each temperature spectrum by the square of the local mean adiabatic temperature gradient. This assumption is better at lower wave numbers and more suspect at higher wave numbers, which may be contaminated by the effects of fine structure. A comprehensive analysis of the effects of temperature fine structure in these measurements is given by *Levine and Irish* [1981]. The most energetic spectrum is the shallowest, with energy decreasing with increasing depth. The

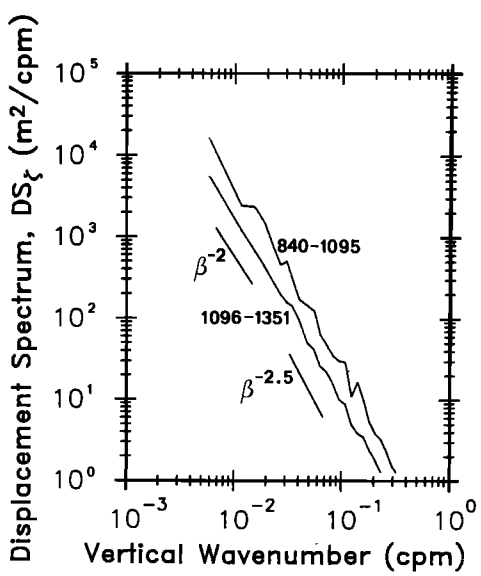

Fig. 4. Vertical wave number spectra of vertical displacement DS_ζ calculated from temperature profiles measured with the CTDSV over depth ranges of 840–1095 and 1096–1351 m. The vertical displacement is inferred from temperature by assuming a constant vertical adiabatic temperature gradient of 1.9×10^{-3} °C/m.

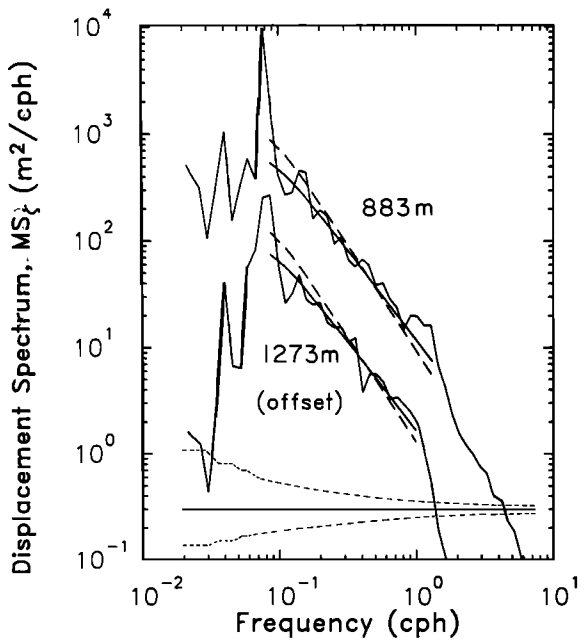

Fig. 5. Frequency spectra of vertical displacement MS_ζ observed from temperature sensors on A2 at 883 m (no offset) and 1273 m (offset by a factor of 0.1). The vertical displacement is inferred from temperature by assuming a constant vertical adiabatic temperature gradient of 2.00×10^{-3} °C/m at 883 m and 1.62×10^{-3} °C/m at 1273 m. The data are compared with the MATE model (solid line) and the GM model (dashed line). The 95% confidence limits are also indicated.

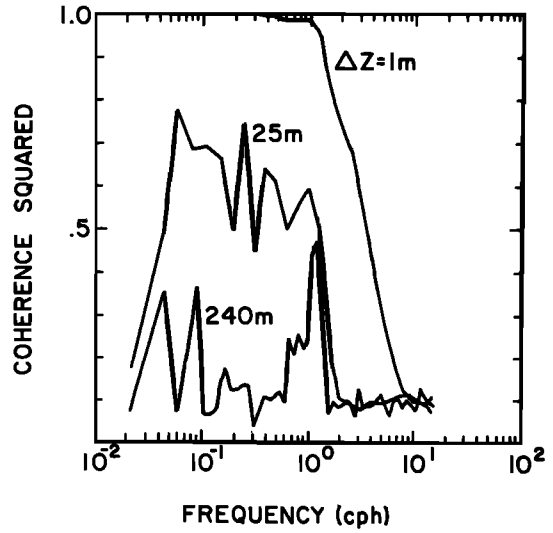

Fig. 6*a*

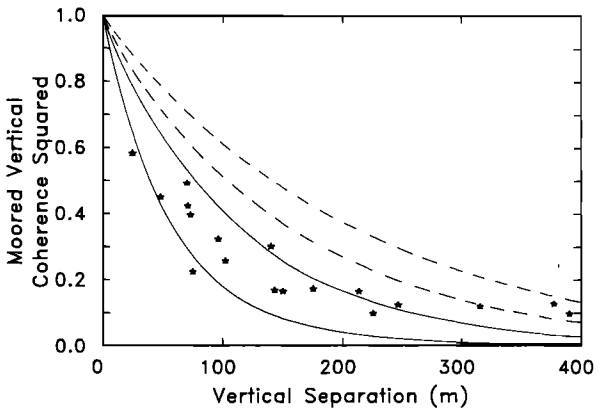

Fig. 6*b*

Fig. 6. The vertical coherence of vertical displacement MVC_ζ observed by temperature sensors on A2. (*a*) MVC_ζ as a function of frequency for vertical separation of 1, 25, and 240 m. (*b*) The average level of the MVC_ζ in the internal wave band (0.2–0.7 cph) as a function of vertical separation. The data are compared (stars) with the MATE model for the range of $t = 2.5$ to 3.6 m^{-1} s for $N = 1.0$ to 1.35 cph (between solid lines) and the GM model with $t = 1.4$ m^{-1} s for $N = 1.0$ to 1.35 cph (between dashed lines).

spectra drop at $\beta^{-2.1}$ from 6×10^{-3} cpm to about 6×10^{-2} cpm, then fall faster at about $\beta^{-2.6}$.

Moored Temperature Arrays

The two temperature arrays were designed as taut moorings with all buoyancy at 400 m, below the influence of the wind wave field. The top sensor on each array was an Aanderaa current meter measuring horizontal velocity and temperature; the other sensors, 18 temperature (Sea-Bird Electronics), two conductivity (Sea-Bird Electronics), and two pressure (Vibrotron), were divided equally between the arrays (Figure 2). Acoustic transponders on the arrays allowed shipboard tracking; A1 was positioned 332 m southeast of A2.

The pressure records show the mean depth, tidal fluctuations, and array motion. The amplitude of the pressure fluctuations recorded on A2 agrees to within 1/4 m of the barotropic tide predicted from previous measurements on Cobb Seamount [*Larsen and Irish*, 1975]. Therefore the vertical excursion of the sensors is neglected. However, the vertical motion of A1 having 1/3 the buoyancy of A2 may not be negligible. Hence most results will be based on data from A2.

Frequency spectra were calculated from all the moored temperature records. A linear trend was removed from each series and a cosine taper applied to the first and last 10% of the series to correct for end-effects, as suggested by *Bingham et al.* [1967]. The temperature spectra were converted to vertical displacement spectra by dividing by the square of the local average adiabatic temperature gradient. Examples of moored vertical displacement spectra (MS_ζ) corrected for sensor response are shown in Figure 5.

The energy below the inertial frequency ($f = 1.06 \times 10^{-4}$ s^{-1}) is attributed to the advection of temperature structure by low-frequency currents as well as the internal wave field itself [*Levine and Irish*, 1981]. The dominant energy is tidal; significant peaks are present at both the diurnal and semidiurnal frequencies. As typically observed in internal wave spectra, there is a sharp rise at f followed by a smooth spectral roll-off. Near N there is a sharp break in slope with an $\omega^{-2.5}$ dependence above N.

Estimates of the coherence in frequency space between vertically separated sensors (moored vertical coherence, MVC_ζ) are shown in Figure 6. Each temperature record was divided into 50% overlapping blocks as suggested by *Carter et al.* [1973]. A linear trend was removed and a cosine taper applied to the first and last 10% of each block. Cross-spectral estimates were formed by ensemble averaging the blocks, and coherences were estimated by normalizing by the appropriate autospectra. For the three vertical separations shown in Figure 6*a*, the coherence in the internal wave band decreases with increasing separation. There are peaks at the tidal and buoyancy frequencies for separations of 25 and 240 m. Above the local buoyancy frequency, the coherence drops to a bias level that is statistically indistinguishable from zero. Since there is significant variation of coherence with frequency, the average coherence in the band between 0.2 to 0.7 cph was

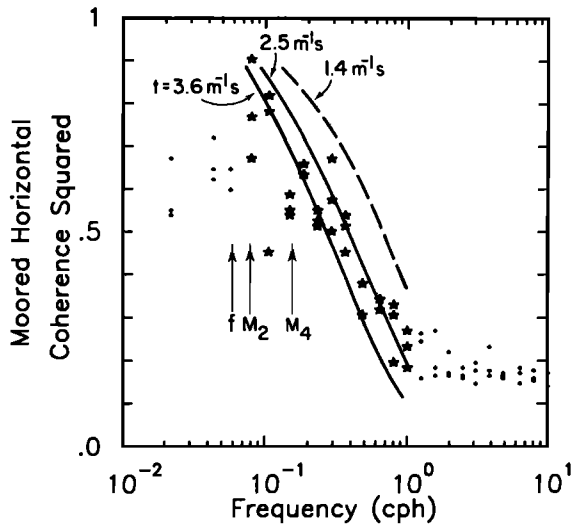

Fig. 7. The horizontal coherence of vertical displacement MHC_ζ between three pairs of temperature sensors on A1 and A2 separated horizontally by 332 m at nearly the same depth. Values in the internal wave frequency band (stars) are compared with the MATE model (solid lines) and the GM model (dashed line).

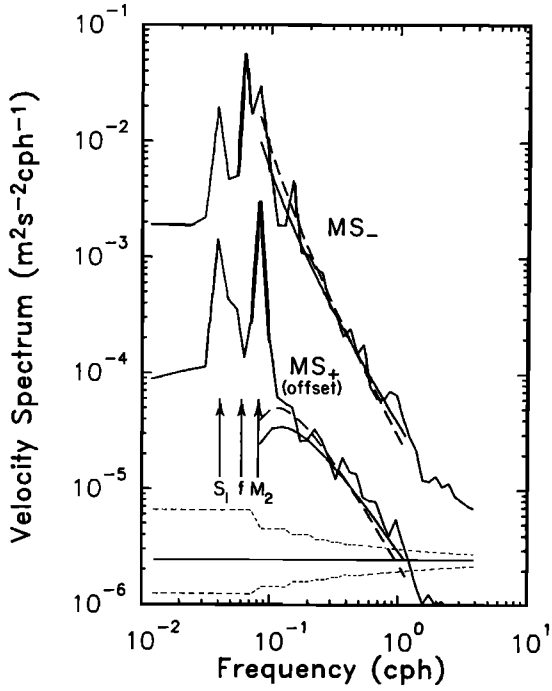

Fig. 8. Frequency spectra of the clockwise MS_- and the counterclockwise MS_+ (offset by a factor of 0.1) components of horizontal velocity observed from C1 at 1079 m. The data are compared with the MATE model (solid line) and the GM model (dashed line). The 95% confidence limits are also indicated.

calculated and plotted as a function of vertical separation in Figure 6*b*.

The coherence in frequency space between sensors horizontally separated on A1 and A2 (moored horizontal coherence, MHC_ζ) was calculated in a manner similar to the MVC_ζ. The coherence was estimated between pairs of sensors moored at nearly the same depth at the horizontal separation of 332 m (Figure 7). There is significant coherence above f to nearly 1 cph, where the coherence falls to the bias level.

Moored Current Meter Array

The current meter array consisted of four Aanderaa current meters. The array was less buoyant than either of the temperature arrays, and hence larger array motion was expected. Because there was no pressure sensor on this array, the magnitude of the vertical motion is unknown. The location of the array, which had no tracking transponder, was estimated to be about 500 m west of A2.

Spectra were calculated using the rotary representation of the velocity vector. Representative rotary spectra from 1079 m (MS_+ and MS_- for the counterclockwise and clockwise components, respectively) are shown in Figure 8. There is a sharp peak at the inertial frequency as well as at the diurnal and semidiurnal tidal frequencies. The inertial peak is the largest and is almost entirely in the clockwise component as expected. An additional peak is seen at 0.14 cph, at about twice the inertial frequency. This peak is not an exact harmonic of either the inertial peak (which is observed at a slightly higher frequency than f) or the semidiurnal tidal frequency, and its origin is unknown. Above f, the spectra fall off smoothly toward N, where there is a slight but significant break in slope. Approaching N, the MS_+ and MS_- are nearly the same. Above the fall-off at N, the velocity spectra become whiter due to the effects of spectral aliasing, current fine structure, and/or array motion.

SPURV

Horizontal temperature profiles were measured by running SPURV along an isobaric trajectory (1184 dbars). In the region midway between the two seamounts, two 11-km legs were made at right angles (west-to-east followed by north-to-south) to test horizontal isotropy. The horizontal wave number spectra (towed spectra, TS_ζ) for the two legs are shown in Figure 9 using an equivalent vertical displacement scale based on the mean vertical adiabatic temperature gradient. The spectra were truncated at a wave number where sensor response and digitizing effects become dominant. At low wave number the spectra exhibit an α^{-2} dependence. At 0.03 cpm there is a break in slope followed by an $\alpha^{-1.6}$ dependence at higher wave number. The lack of any significant difference between the spectra is consistent with a horizontally isotropic wave field.

Two temperature sensors attached to SPURV and separated vertically by 0.94 m measured the coherence in horizontal wave number space (towed vertical coherence, TVC_ζ). The TVC_ζ was calculated for the two legs, using the same method described for the MVC_ζ, and plotted in Figure 10. The results from the north-south and east-west legs are statistically identical. The TVC_ζ is near 1 at low wave numbers and drops to near zero above 0.01 cpm.

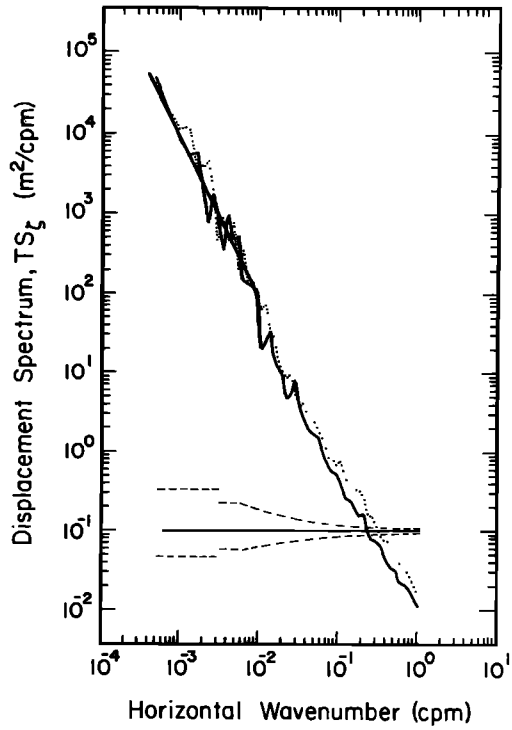

Fig. 9. Horizontal wave number spectra of vertical displacement TS_ζ observed by SPURV during horizontal runs oriented north to south (solid line) and west to east (dotted line) at 1184 dbar. The vertical displacement is inferred from temperature by assuming a constant vertical adiabatic temperature gradient of 1.64×10^{-3} °C/m. The best fit to α^{-2} over the wave number band 4.7×10^{-4} to 9.0×10^{-3} cpm is shown by a straight solid line. The 95% confidence limits are also shown.

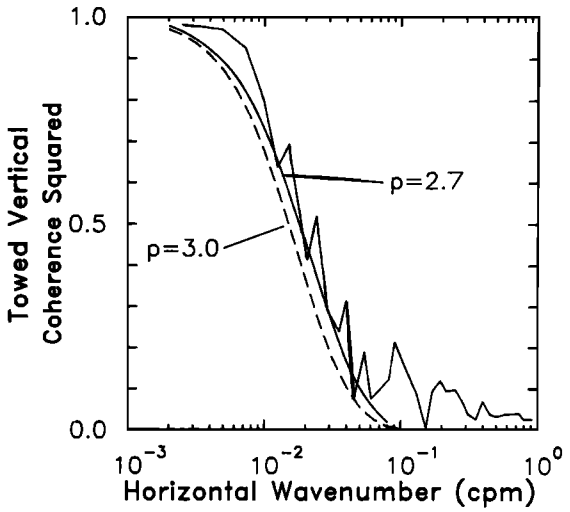

Fig. 10. The horizontal wave number coherence of vertical displacement TVC_ζ between a pair of temperature sensors separated vertically by 0.94 m on SPURV. The data are compared with the MATE model (section 5) with $p = 2.7$ (solid line) and the GM model with $p = 3.0$ (dashed line).

3. Consistency Relations

Internal wave consistency relationships express constraints between the horizontal velocity and vertical displacement fields at a single point. Although there are only a few general relations, they are worth examining because they are independent of the specific spectral composition of the wave field. Two independent consistency relationships are applied to the MATE data set. These expressions are valid for a sum of any number of waves of different wave numbers; the wave field is not restricted to be horizontally or vertically isotropic. The derivations hinge on the assumptions that the wave field is linear and each wave component is independent.

The first, originally presented by *Fofonoff* [1969], relates the potential energy to horizontal kinetic energy:

$$\frac{N^2 \mathrm{MS}_\zeta(\omega)}{\mathrm{MS}_u(\omega) + \mathrm{MS}_v(\omega)} = \frac{N^2}{N^2 - \omega^2} \frac{\omega^2 - f^2}{\omega^2 + f^2} \tag{1}$$

As $\omega \to f$, the vertical displacement goes to zero, and as $\omega \to N$, the horizontal velocity becomes negligible. To compare with measurements made at various values of $N(z)$, the equation is rewritten

$$\frac{N^2 \mathrm{MS}_\zeta(\omega)}{\mathrm{MS}_u(\omega) + \mathrm{MS}_v(\omega)} \frac{N^2 - \omega^2}{N^2} = \frac{\omega^2 - f^2}{\omega^2 + f^2} \tag{2}$$

The left-hand side can then be estimated from data and compared with the right-hand side.

The other expression relates the ratio of the counterclockwise to clockwise components of the rotary spectrum

$$\frac{\mathrm{MS}_+}{\mathrm{MS}_-} = \frac{(\omega - f)^2}{(\omega + f)^2} \tag{3}$$

This relation is a variation of the "rotary coefficient" originally derived by *Gonella* [1972].

These relationships are compared with data from the four current meters on C1 and the one on top of A2. The observed ratio of potential to kinetic energy is plotted with the theoretical relation (2) in Figure 11*a*. The amount of scatter of the data is reasonable when compared with the confidence limits.

The observed ratio of the rotary spectra $\mathrm{MS}_+/\mathrm{MS}_-$ is plotted with the theoretical result in Figure 11*b*. At high frequency the agreement is good; however, this is not a very sensitive test for internal waves, since the ratio for random noise is also 1. Below about 0.16 cph there are significant deviations from the theory. One explanation is that the many waves of different horizontal wavelengths (modes) at tidal frequency are not statistically independent. If the nearby seamounts are a source of internal tide, then it is reasonable to expect the various wave numbers of the internal tide to be correlated, thereby violating one of the assumptions used in deriving (3).

4. Spectral Model

We introduce a modified form of the Garrett-Munk internal wave model as a framework for comparing the variety of spatial and temporal measurements made during MATE. The primary alteration of the GM model is a generalization of the frequency dependence of the spectrum by adding a parameter p, which specifies the frequency spectral slope. This modification permits a closer comparison of the observations with the model. Some of the GM parameters are redefined to identify explicitly the total energy, frequency dependence, and depth scaling in the analytical expressions of the spectral quantities.

The moored spectra of both vertical displacement MS_ζ and

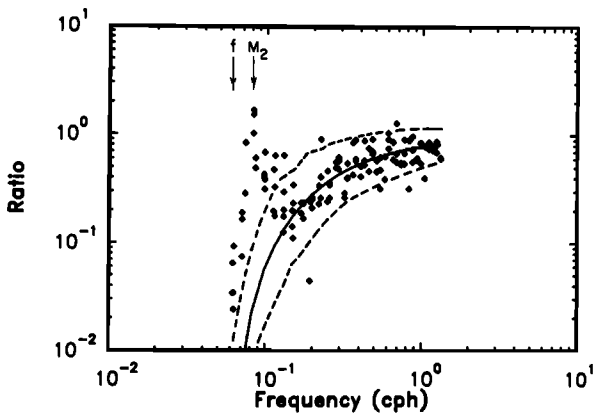

Fig. 11*a*

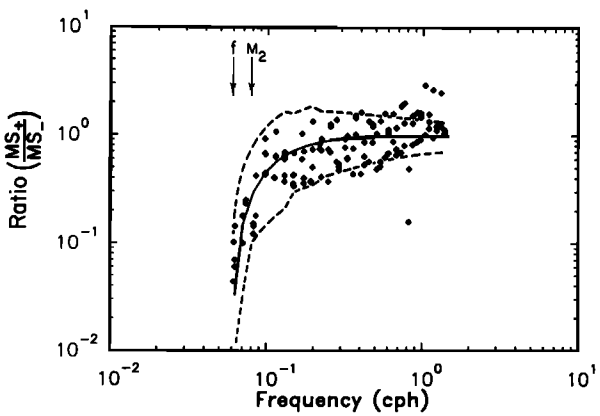

Fig. 11*b*

Fig. 11. (*a*) The ratio of potential to horizontal kinetic energy and (*b*) the ratio of counterclockwise to clockwise components of horizontal velocity are compared with the theoretical relationships (solid line). The data are from the four current meters on C1 and the one on top of A2. The 95% confidence limits (dashed lines) are also shown.

horizontal velocity MS_u are written in the following form:

$$MS_u(\omega) = MS_v(\omega) = \frac{\tilde{E}}{2}\left(\frac{N(z)}{\tilde{N}}\right)\left(\frac{(\Omega^2+1)(\Omega^2-1)^{-1/2}\Omega^{-p}}{Jf}\right) \quad (4)$$

$$MS_\zeta(\omega) = \tilde{E}\left(\frac{1}{N(z)\tilde{N}}\right)\left(\frac{(\Omega^2-1)^{1/2}\Omega^{-p}}{Jf}\right) \quad (5)$$

where $\Omega = \omega/f$. These expressions can easily be derived from the GM formulation [e.g., *Munk*, 1981]. The first bracketted factor on the right-hand side of (4) and (5) represents the depth scaling referenced to frequency $\tilde{N}$ (modified WKB approximation used by GM). The quantity $\tilde{E}$ is the total internal wave energy per unit mass scaled to the reference frequency $\tilde{N}$; quantities marked by tildes are referenced to a depth where $N(z) = \tilde{N}$. We choose $\tilde{N}$ to be 1.74×10^{-3} s^{-1} (1 cph), a reasonable scale in the deep ocean. The choice of $\tilde{N}$ is not critical, as it just serves as a common reference to compare measurements made at different buoyancy frequencies. The second bracketted term contains the frequency dependence as given by GM with the addition of the parameter p (in the GM model $p = 3$). At frequencies much greater than f, both MS_u and MS_ζ have ω^{-p+1} frequency dependence. The nondimensional normalization factor J is defined so that the total internal wave energy per unit mass (J/kg) over all frequencies at a local buoyancy frequency of $N(z)$ is given by

$$\tilde{E}[N(z)/\tilde{N}] = \frac{1}{2}\int_f^N [MS_u + MS_v + N^2 MS_\zeta]\, d\omega \quad (6)$$

explicitly,

$$J = \int_1^{N/f} \Omega^{2-p}(\Omega^2-1)^{-1/2}\, d\Omega \quad (7)$$

Note that the contribution to the kinetic energy from the vertical velocity has been neglected in accordance with the approximation $(N^2 - \omega^2) \sim N^2$ assumed by GM (for a discussion of the model for $\omega \sim N(z)$, see *Desaubies* [1975]).

The energy $\tilde{E}$ is related to the parameters of the GM model by equating total energy per unit mass [*Munk*, 1981],

$$[\tilde{E}/\tilde{N}]N(z) = [Eb^2 N_0]N(z) \quad (8)$$

$$\tilde{E} = Eb^2 N_0 \tilde{N} \quad (9)$$

where the GM parameter E is the dimensionless energy level, b is the depth scale of $N(z)$, and N_0 is the buoyancy frequency scale. (Note that in the notation of *Desaubies* [1976], $r \equiv Eb^2N_0$; hence $r = \tilde{E}/\tilde{N}$.) Using the GM values of $E = 6.3 \times 10^{-5}$, $b = 1300$ m, and $N_0 = 5.23 \times 10^{-3}$ s^{-1} (3 cph) yields a value of $\tilde{E} = 9.7 \times 10^{-4}$ J/kg.

To describe the partition of energy in wave number space, we choose the analytically convenient functional form of the GM model given by *Desaubies* [1976]. The GM parameter j_*, specifying the equivalent number of vertical modes, always appears in conjunction with other parameters. This combination of parameters has been defined by *Desaubies* [1976]

$$t = \pi j_*/N_0 b \quad \text{m}^{-1}\,\text{s} \quad (10)$$

For the GM value of $j_* = 3$, the quantity $t = 1.39$ m^{-1} s.

The vertical and horizontal wave number spectra of displacement can then be written as

$$DS_\zeta(\beta) = \int_f^N d\omega MS_\zeta(\omega)[(2/\pi)\beta_*(\beta_*^2 + \beta^2)^{-1}] \quad (11)$$

$$TS_\zeta(\alpha) = \int_f^N d\omega MS_\zeta(\omega)\left[(4\alpha_*/\pi^2)\int_\alpha^\infty \frac{d\eta}{(\alpha_*^2+\eta^2)(\eta^2-\alpha^2)^{1/2}}\right] \quad (12)$$

where α_* and β_* are the horizontal and vertical wave number scales given by $t(\omega^2 - f^2)^{1/2}$ and $t(N^2 - \omega^2)^{1/2}$, respectively [*Desaubies*, 1976]. The factors [ ] are the distribution of the energy density in wave number space at frequency ω and are normalized such that the integrals $\int[\ ]d\beta = 1$ and $\int[\ ]d\alpha = 1$. In the TS_ζ the factor [ ] is the sum of the energy contribution to the one-dimensional wave number α from all wave numbers greater than α in a horizontally isotropic wave field. At high wave number, $\beta \gg \beta_*$ and $\alpha \gg \alpha_*$, both spectra are proportional to t for any value of p:

$$DS_\zeta(\beta) = Bt\beta^{-2} \quad (13)$$

$$TS_\zeta(\alpha) = Ct\alpha^{-2} \quad (14)$$

where

$$B = \frac{2}{\pi}\int_f^N (N^2-\omega^2)^{1/2} MS_\zeta(\omega)\, d\omega \quad (15)$$

$$C = (4/\pi^2)\int_f^N (\omega^2 - f^2)^{1/2} MS_\zeta(\omega)\, d\omega \quad (16)$$

Analytical expressions for the GM frequency dependence of $p = 3$ are

$$B = (\tilde{E}/\pi\tilde{N})(1-v)^2 \quad (17)$$

$$C = (8\tilde{E}/\pi^3\tilde{N})v[\tfrac{1}{2}(v^2-1) - \ln v] \quad (18)$$

where $v \equiv f/N$. For arbitrary p, values of C were evaluated analytically, while the integrals needed to calculate B required numerical integration.

The moored vertical and horizontal coherences (MVC_ζ and MHC_ζ) are independent of $\tilde{E}$ and p. These quantities depend only on the parameter t and can be written [*Desaubies*, 1976]

$$MVC_\zeta(\omega) = \exp[-(N^2-\omega^2)^{1/2} t\Delta z] \quad (19)$$

$$MHC_\zeta(\omega) = I_0(H) - L_0(H) \quad (20)$$

where $H = tf(\Omega^2-1)^{1/2}\Delta x$, Δx (Δz) is the horizontal (vertical) separation, I_0 is the modified Bessel function, and L_0 is the Struve function.

The towed vertical coherence (TVC_ζ) is not a function of $\tilde{E}$ or t but in this parameterization depends only upon the vertical separation Δz and the parameter p. Modifying the expression given by *Desaubies* [1976] to include the parameter p, the TVC_ζ can be written

$$TVC_\zeta(\alpha;\Delta z) = \frac{1}{TS_\zeta}\int_f^N d\omega\ MS_\zeta(\omega) \cdot\left[(4\alpha_*/\pi^2)\int_\alpha^\infty \frac{\cos(\theta\eta)\, d\eta}{(\alpha_*^2+\eta^2)(\eta^2-\alpha^2)^{1/2}}\right] \quad (21)$$

where

$$\theta = \Delta z\left(\frac{v^{-2}-\Omega^2}{\Omega^2-1}\right)^{1/2}$$

To evaluation for arbitrary p, numerical integration of the double integral was required.

A summary of the dependences of the statistical quantities on the parameters $\tilde{E}$, t, and p is presented in Table 1.

TABLE 1. Dependences of Statistical Quantities on Model Parameters

	Model Parameter			
	$\tilde{E}$	t	$\tilde{E}t$	p
MS_u	X			X
MS_ζ	X			X
TS_ζ			X	X
DS_ζ			X	X
MVC_ζ		X		
MHC_ζ		X		
TVC_ζ				X

An X indicates that the quantity is a function of that model parameter.

5. Comparison of Data With Spectral Model

In this section the data presented in section 2 are compared with the theoretical formulation presented in section 4. There are three independent parameters, $\tilde{E}$, t, and p, that must be chosen to completely specify the spectral behavior of the model. These parameters are selected to fit in an optimum way the many statistical quantities measured simultaneously during MATE. Because of the variety of measurements, several independent determinations of each parameter are possible. Both MS_ζ and MS_u provide estimates of $\tilde{E}$, the moored vertical and horizontal coherences (MVC_ζ and MHC_ζ) allow estimation of t, and the DS_ζ and TS_ζ yield values of the product $\tilde{E}t$ (Table 1). These quantities are all dependent upon p. The value of p can be determined directly from the slope of the frequency spectra of velocity and displacement; the TVC_ζ is also a function of p independent of $\tilde{E}$ and t. Consistency among estimates of $\tilde{E}$, t, and p is then used to verify the behavior of the model.

Estimates of $\tilde{E}$ from moored spectra are found by minimizing the squared difference ε^2 between the logarithm of the observed spectrum and the logarithm of the model spectrum. Specifically,

$$\varepsilon^2 = \frac{1}{MK} \sum_{k=1}^{K} \sum_{m=1}^{M} \left(\frac{\log S_{\text{obs}}(z_k, \omega_m) - \log S_{\text{model}}(z_k, \omega_m)}{\log [L(\omega_m)]} \right)^2 \tag{22}$$

where $S_{\text{obs}}(z_k, \omega_m)$ and $S_{\text{model}}(z_k, \omega_m)$ are the observed and model spectra, respectively, at depth z_k over a frequency band centered at ω_m. The function S_{model} for vertical displacement is MS_ζ (5) and for total horizontal velocity is $MS_u + MS_v$ (4). The quantity ε^2 is the average squared error over M frequency bands and K depths. The function $L(\omega_m)$ is the length of the 95% confidence band of S_{obs}; its purpose is to give more weight to spectral estimates of higher statistical confidence [*Levine et al.*, 1983].

The best fit values of $\tilde{E}$ as a function of p are shown in Figure 12*a*. These results are based on data from seven depths for displacement and five depths for velocity (883–1273 m). The fit is made over the internal wave frequency band from 0.2 to 0.7 cph; this is the center of the continuum away from the buoyancy frequency and the internal tide. The minimum squared error ε^2 occurs at $p = 2.5$–2.7 for displacement and $p = 2.65$–2.85 for velocity, although the precise locations of the minima are somewhat vague (Figure 12*a*). As a compromise, the value of $p = 2.7$ is chosen for overall best fit, and the spectral models of both displacement and velocity for this value are plotted with the observed spectra in Figures 5 and 8. It is clear from the figures that the spectral slope of $p = 2.7$ is a better fit than the $p = 3$ of the GM model. The TVC_ζ also provides an estimate of p independent of $\tilde{E}$ and t. The coher-

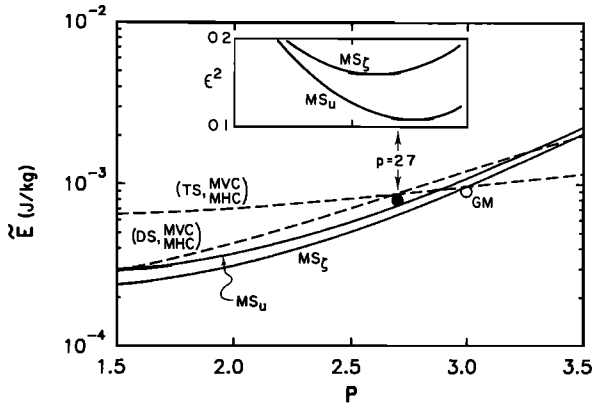

Fig. 12*a*

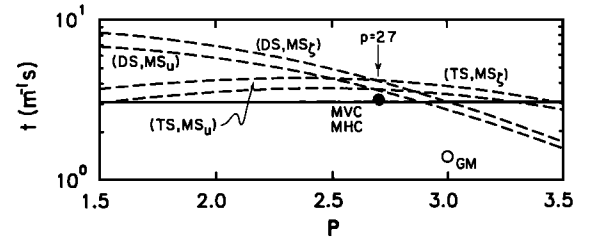

Fig. 12*b*

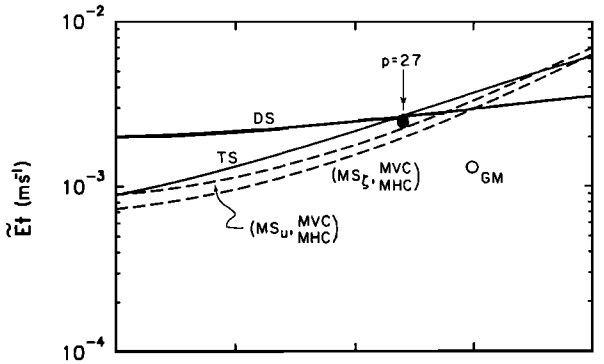

Fig. 12*c*

Fig. 12. Estimates of the model parameters $\tilde{E}$, $\tilde{E}t$, and t from the MATE data. The overall best fit values are shown as solid circles; for comparison, the GM values are also indicated (open circles). (*a*) The best fit values of $\tilde{E}$ as a function of p. Direct estimates from spectra of vertical displacement MS_ζ and horizontal velocity MS_u are shown as solid lines. Indirect estimates of $\tilde{E}$ using direct estimates of $\tilde{E}t$ from DS_ζ and TS_ζ, and t from MVC and MHC are shown as dashed lines. The squared error ε^2 (22) of the fit is shown in the inset. (*b*) The best fit values of t as a function of p. Direct estimates from vertical and horizontal coherences, MVC and MHC, are shown as a solid line. Indirect estimates of t using direct estimates of $\tilde{E}t$ from DS_ζ and TS_ζ, and $\tilde{E}$ from vertical displacement and horizontal velocity spectra, MS_ζ and MS_u, are shown as dashed lines. (*c*) The best fit values of $\tilde{E}t$ as a function of p. Direct estimates from vertical and horizontal wave number spectra, DS_ζ and TS_ζ, are shown as solid lines. Indirect estimates of $\tilde{E}t$ using direct estimates of $\tilde{E}$ from MS_ζ and MS_u, and t from MVC and MHC are shown as dashed lines.

ence data compare more favorably with the value of $p = 2.7$ than the GM model value (Figure 10).

The MVC_ζ and MHC_ζ are used to determine the best value of t, since they are both independent of p and $\tilde{E}$. The model MVC_ζ is also independent of frequency. Even though the observed MVC_ζ show significant fluctuations in frequency (Figure 6*a*), average values for the band 0.2–0.7 cph were calculated to compare with the model for all possible vertical separations (Figure 6*b*). At large vertical separations the coherence squared approaches the bias level; estimates near 0.1 are not significantly different from zero. The model results (19) are also plotted in Figure 6*b* for a range of values of $t = 2.5$–3.6 m^{-1} s and $N = 1.74$–2.35×10^{-3} s^{-1} (1.0–1.35 cph); the GM value of $t = 1.39$ m^{-1} s ($j_* = 3$) is also shown. While there is large scatter in the data, it is clear that $t = 2.5$–3.6 m^{-1} s fits better than the GM values. The model MHC_ζ (20) is compared with the observations at the only horizontal separation of 332 m in Figure 7. The data are less coherent at a given frequency than predicted by the GM model. The observed horizontal coherences are remarkably consistent with the same range of t of 2.5–3.6 m^{-1} s that fits the vertical coherences. Although it is difficult to estimate a precise value of t from these coherences, the average value of 3.1 m^{-1} s is plotted in Figure 12*b* along with the GM result.

The product $\tilde{E}t$ is estimated independently from the level of the TS_ζ, from horizontal profiles made by SPURV, and the DS_ζ, from vertical profiles made with the CTDSV. To fit the TS_ζ, the model spectral shape α^{-2} (14) was fit to the observations, minimizing a squared error defined in an analogous manner to (20) over the wave numbers 4.7×10^{-4} to 9.0×10^{-3} cpm (Figure 9). The fit was not extended beyond 10^{-2} cpm because the wave number dependence of the spectrum changes, and these wavelengths are probably too small to be modeled reasonably by a linear model. The estimates of $\tilde{E}t$ are plotted as a function of p in Figure 12*c*. A similar approach could be used to obtained $\tilde{E}t$ from the DS_ζ; however, instead we use the results from the detailed analysis of *Levine and Irish* [1981]. They used the same data set and included the effects of temperature fine structure in the presence of the internal wave field. It was found that approximately 1/2 of the DS from wave numbers 0.004 to 0.05 cpm at 1013-m depth was caused by internal waves, while the remainder was temperature fine structure. Estimates of $\tilde{E}t$ were obtained using their value for the level of the uncontaminated DS_ζ and are also plotted in Figure 12*c*.

The consistency among the independent estimates of $\tilde{E}$, t, and the product $\tilde{E}t$ can be checked, since any two quantities can be used to calculate the third. Direct estimates of $\tilde{E}t$ from TS_ζ and DS_ζ (Figure 12*c*) and $t = 3.1$ m^{-1} s from the MVC_ζ and MHC_ζ (Figure 12*b*) yield indirect estimates of $\tilde{E}$, plotted as a dashed line in Figure 12*a*. Similarly, the indirect estimates of $\tilde{E}t$, from direct estimates of $\tilde{E}$ and t, are displayed in Figure 12*c*, and indirect estimates of t, from direct estimates of $\tilde{E}t$ and $\tilde{E}$, are shown in Figure 12*b*. The agreement is remarkably good among all the measurements for $p = 2.7$—better than a factor of 2.

6. Discussion

To put the observations made during MATE into perspective, we briefly survey the historical set of internal wave observations. The major features of the wave field as observed in most internal wave studies can be reasonably described by the GM spectrum. The GM model serves as a benchmark that can easily be related to other observations. Systematic discussions of the historical data are presented by *Wunsch* [1976], *Wunsch and Webb* [1979], *Roth et al.* [1981], and *Levine et al.* [1985].

In terms of total energy per unit volume, the internal wave field during MATE agrees with the GM level and falls in the middle among historical values [*Levine et al.*, 1985]. Near steep topographic features such as Muir Seamounts, Hydrographer Canyon [*Wunsch*, 1976], and Hudson Canyon [*Hotchkiss and Wunsch*, 1982] the energy in the wave fields is significantly higher by a factor of 2–50 than the GM level. At MATE the effect of the nearby seamounts (9 km away) on the background energy is apparently not significant.

The frequency spectral slope ω^{-p+1} in the internal wave band at $\omega > f$ was found to be consistent with $p = 2.7$. This is slightly less steep than the canonical GM value of $p = 3$. However, other studies have noted that a dependence less steep than ω^{-2} generally fits moored spectral data better [e.g., *Wunsch*, 1976; *Levine et al.*, 1983]. The modified GM model allows the variation of the parameter p to be tested by all relevant statistical quantities, not just the slope of the frequency spectrum itself; there is significant improvement between data and theory at MATE with $p = 2.7$.

The parameter t, which is directly related to the equivalent number of modes j_*, sets the wave number bandwidth in the GM model. At MATE the best fit value of $t = 3.1$ m^{-1} s ($j^* = 6$) is a factor of 2 higher than the canonical GM value. There are not many accurate determinations of t, so the number of good comparisons are limited. The best comparison is with the results from the extensive measurements made during the Internal Wave Experiment (IWEX) [*Briscoe*, 1975; *Müller et al.*, 1978]. The IWEX model allows t to be a function of frequency. To examine results from models with slightly different parameterizations, it is most useful to use "equivalent bandwidth" when comparing results [see *Müller et al.*, 1978, p. 492]. The IWEX results, when converted to units of t, show a decrease from $t = 3.3$ m^{-1} s ($j_* = 6.4$) at low frequency to $t = 1.7$ m^{-1} s ($j_* = 3.2$) near N. In the frequency band where the MATE data were fit, above the tide and below N, the IWEX value of $t = 2.4$ m^{-1} s ($j_* = 4.7$) falls between the MATE and GM value. If a value of t had been estimated at high-frequency near N for MATE, a lower value of t would result due to the high coherence near N (Figure 6). This feature is consistent with the decrease in t at high frequency in the IWEX model.

The modfied GM model presented here is still admittedly crude—only three parameters to define the statistics of the internal wave field. However, it does permit a more accurate representation of the internal wave field at MATE than the GM model. The formalism can also be applied to other observations where the frequency spectral slope differs from ω^{-2}.

The spectral description of the internal waves at MATE may provide useful information to theoreticians seeking the best kinematic formulation of the wave field to test theories of internal wave dynamics. During the last 10 years there has been considerable effort in trying to understand the dynamics of a random sea of internal gravity waves. A variety of theoretical techniques have been used to study nonlinear interactions among internal waves (see *West* [1981] and *Müller et al.* [1986] for reviews of the topic). To relate their results to the ocean, some form of the GM model is usually used as the base state of the oceanic internal wave field. Transfers among wave components in frequency/wave number space by nonlinear interaction are then estimated. If a different base state of the

internal wave field were chosen, such as that found during MATE, then some of the theoretical results may be modified. However, due to the complexity of these theories, further investigation is necessary to determine if the modifications would be significant.

Little has been mentioned about the effect of noninternal wave fine structure on the results of this analysis. From the detailed study of temperature fine structure by *Levine and Irish* [1981], we conclude that the moored vertical displacement spectrum MS_ζ is essentially uncontaminated by fine structure. The internal wave signal was found to be a factor of 10 higher than the fine structure contamination in the internal wave frequency band; this agrees quantitatively with the results from IWEX [*Müller et al.*, 1978]. The moored vertical coherences MVC_ζ also were found to be unaffected by fine structure at vertical separations greater than 10 m. However, the effects of fine structure are significant at high wave numbers in estimates of dropped spectra DS_ζ inferred from temperature measurements, and this effect has been taken into account. No estimate of the importance of current fine structure in the velocity observations has been made. However, if we apply the results from IWEX to the MATE data, then the contamination in the moored velocity spectrum MS_u is a factor of 2–3 below the internal wave signal over most of the internal wave frequency band. Near N, however, the fine structure effects may actually dominate. If one uses this estimate of current fine structure and removes it from our spectral estimates, the effect on the overall fit would be relatively small and would not significantly affect our conclusions.

7. Summary and Conclusion

The unique feature of the MATE internal wave study was the acquisition of towed and dropped measurements simultaneously with moored observations. This permits careful examination of internal wave statistics in frequency and vertical and horizontal wave number. A generalized formulation of the Garrett-Munk spectral model was used as a framework for comparing these diverse observations. In this modified version of the GM model, three parameters, p, $\tilde{E}$, and t, are needed to specify the entire spectral behavior. The parameter p sets the frequency dependence; the spectral behavior for both horizontal velocity and vertical displacement is ω^{-p+1} at $\omega > f$. The quantity $\tilde{E}$ is the total energy of the internal wave field per unit mass at the reference buoyancy frequency $\tilde{N}$; it appears as a factor in the expression for all spectral quantities ((4), (5), (11), (12)). We choose the value of $\tilde{N} = 1.74 \times 10^{-3}$ s^{-1} (1 cph) as a reasonable scale. The parameter t sets the wave number bandwidth of the wave field, thereby controlling the spatial coherence scales and the vertical and horizontal wave number spectra. Expressed in terms of the GM parameters E, b, and j_*,

$$\tilde{E}/\tilde{N} = Eb^2N_0$$

$$t = \pi j_*/N_0 b$$

This model would be useful to apply to other observations where the value of p differs from the GM value.

Independent observations made during MATE were used to determine $\tilde{E}$, t, and the product $\tilde{E}t$, directly. The best fit of the data to the spectral model is summarized in Figure 12 as a function of p. The directly determined value of $\tilde{E}$, from moored spectra of displacement and velocity, had the least error ε^2 for a value of $p = 2.7$, significantly less than the GM value of $p = 3$ (Figure 12*a*). However, the value of $\tilde{E} = 8 \times 10^{-4}$ J/kg at $p = 2.7$ is in good agreement with the GM model (about 10% lower). Indirectly inferred values of $\tilde{E}$ from estimates of t and $\tilde{E}t$ from coherences and wave number spectra are consistent with the directly measured $\tilde{E}$ (Figure 12*a*).

The directly determined value of t from the moored coherences is independent of p and estimated to be 3.1 m^{-1} s (Figure 12*b*). This is about a factor of 2 larger than the GM value (equivalent to a $j_* = 6$ in the GM model). Indirectly inferred values of t from directly determined $\tilde{E}t$ and $\tilde{E}$ are consistent and distinctly higher than the GM level.

Direct measurements of $\tilde{E}t$ from both vertical and horizontal wave number spectra are nearly equal at $p = 2.7$ (Figure 12*c*). Indirect estimates are consistent and about twice the GM value.

An independent verification of the parameterization of the internal wave field is provided by the acoustic experiment. MATE was a unique experiment, designed to test our ability to relate observed internal wave fluctuations to simultaneously measured acoustic variability. The acoustic experiment consisted of observations of pulses at 2, 4, 8, and 13 kHz, transmitted over a fixed 18.1-km path between towers anchored on the two seamounts. The data were reduced to time series of pulse amplitude and travel time. The temporal fluctuations of the acoustic signals were due primarily to the oscillations of the sound speed field caused by tides, internal waves, and fine structure. The statistical description of the internal wave field presented here is used as input to acoustic theories, which can then be verified using the observed amplitude and travel time statistics. The observed travel time fluctuations agree well with the predictions using the description of the internal waves provided by the MATE model [*Ewart and Reynolds*, 1984]. There is significant improvement using the spectral slope $p = 2.7$ and bandwidth $t = 3.1$ m^{-1} s ($j_* = 6$) compared with the cannonical GM values. This independent sampling of the wave field increases confidence in the validity of the MATE model.

There are perhaps two perspectives with which to view these results. The internal wave specialist would stress the deviations from the GM model: (1) frequency spectral slope $\omega^{-1.7}$ ($p = 2.7$) at high frequency rather than ω^{-2} ($p = 3$) and (2) value of t about twice the GM value ($j_* = 6$). Certainly deviations from the GM model, of this magnitude and larger, have been reported previously [e.g., *Wunsch and Webb*, 1979]. But often only one or two types of measurements are available, and usually it cannot be determined if the deviations are consistent with internal waves or due to some other processes. Because of the variety of towed, dropped, and moored observations at MATE, the parameters were evaluated from independent measurements and found to be consistent with the kinematics of internal waves.

The generalist would note that the observations are still remarkably similar to the GM "universal" spectrum that was originally derived from fits to data taken at vastly different times and places. From this viewpoint the experiment can be seen as contributing another piece of evidence to better define the internal wave climatology. It is perhaps surprising that the deviations are so small given that MATE was a single experiment lasting less than 1 month in a unique topographic setting.

Acknowledgments. We profited from the advice and help of our colleague Yves Desaubies. The technical assistance of Le Olson and Art Pederson made the experiment a success. Thanks are also due to all the other MATE participants from the Applied Physics Labora-

tory, University of Washington, and the officers and crew of the USNS *DeSteiguer*. MATE was funded by the Office of Naval Research (contract N00017-74-C-1208) and the Naval Sea Systems Command (contract N00017-71-C-1305). Support for M. Levine for manuscript preparation was supplied by the Office of Naval Research under contracts N00014-79-C-0004 and N00014-84-C-0218.

REFERENCES

Baines, P. G., On internal tide generation models, *Deep Sea Res.*, *29*, 307–338, 1982.

Bingham, C., M. D. Godfrey, and J. W. Tukey, Modern techniques of power spectrum estimation, *IEEE Trans. Audio Electroacoust.*, *2*, 56–66, 1967.

Briscoe, M. G., Preliminary results from the tri-moored Internal Wave Experiment (IWEX), *J. Geophys. Res.*, *80*, 3872–3884, 1975.

Carter, G. C., C. H. Knapp, and A. H. Nuttall, Estimation of the magnitude-squared-coherence function via overlapped fast Fourier transform processing, *IEEE Trans. Audio Electroacoust.*, *AU-21*, 337–344, 1973.

Desaubies, Y. J. F., A linear theory of internal wave spectra and coherences near the Vaisala frequency, *J. Geophys. Res.*, *80*, 895–899, 1975.

Desaubies, Y. J. F., Analytical representation of internal wave spectra, *J. Phys. Oceanogr.*, *6*, 976–981, 1976.

Eriksen, C. C., Observations of internal wave reflection off sloping bottoms, *J. Geophys. Res.*, *87*, 525–538, 1982.

Ewart, T. E., Acoustic fluctuations in the open ocean—A measurement using a fixed refracted path, *J. Acoust. Soc. Am.*, *60*, 46–59, 1976.

Ewart, T. E., and S. A. Reynolds, The mid-ocean acoustic transmission experiment, MATE, *J. Acoust. Soc. Am.*, *75*, 785–802, 1984.

Ewart, T. E., J. D. Irish, and L. O. Olson, The MATE experiment—A preliminary report, *APL-UW Tech. Note 7-77*, Appl. Phys. Lab., Univ. of Wash., Seattle, 1977.

Fofonoff, N., Spectral characteristics of internal waves in the ocean, *Deep Sea Res.*, *16*, 58–71, 1969.

Garrett, C. J. R., and W. H. Munk, Space-time scales of internal waves, *Geophys. Fluid Dyn.*, *2*, 225–264, 1972.

Garrett, C. J. R., and W. H. Munk, Space-time scales of internal waves: A progress report, *J. Geophys. Res.*, *80*, 291–297, 1975.

Gonella, J., A rotary-component method for analyzing meteorological and oceanographic vector time series, *Deep Sea Res.*, *19*, 833–846, 1972.

Hotchkiss, F. S., and C. Wunsch, Internal waves in Hudson Canyon with possible geological implications, *Deep Sea Res.*, *29*, 415–442, 1982.

Larsen, L. H., and J. D. Irish, Tides at Cobb Seamount, *J. Geophys. Res.*, *80*, 1691–1695, 1975.

Levine, M. D., Internal waves in the ocean: A review, *Rev. Geophys. Space Phys.*, *21*, 1206–1216, 1983.

Levine, M. D., and J. D. Irish, A statistical description of temperature fine structure in the presence of internal waves, *J. Phys. Oceanogr.*, *11*, 676–691, 1981.

Levine, M. D., R. A. de Szoeke, and P. P. Niiler, Internal waves in the upper ocean during MILE, *J. Phys. Oceanogr.*, *13*, 240–257, 1983.

Levine, M. D., C. A. Paulson, and J. H. Morison, Internal waves in the Arctic Ocean: Comparison with lower latitude observations, *J. Phys. Oceanogr.*, *15*, 800–809, 1985.

Müller, P., D. J., Olbers, and J. Willebrand, The IWEX spectrum, *J. Geophys. Res.*, *83*, 479–500, 1978.

Müller, P., G. Holloway, F. Henyey, and N. Pomphrey, Nonlinear interactions among internal gravity waves, *Rev. Geophys.*, 24, in press, 1986.

Munk, W. H., Internal waves and small-scale processes, in *Evolution of Physical Oceanography*, edited by B. A. Warren and C. Wunsch, pp. 264–290, MIT Press, Cambridge, Mass., 1981.

Olbers, D. J., Models of the oceanic internal wave field, *Rev. Geophys. Space Phys.*, *21*, 1567–1606, 1983.

Roth, M. W., M. G. Briscoe, and C. H. McComas III, Internal waves in the upper ocean, *J. Phys. Oceanogr.*, *11*, 1234–1247, 1981.

West, B. J. (Ed.), *Nonlinear Properties of Internal Waves*, 351 pp., American Institute of Physics, New York, 1981.

Widditsch, H. R., SPURV, The first decade, *APL-UW Rep. 7215*, Appl. Phys. Lab., Univ. of Wash., Seattle, 1973.

Wunsch, C., Geographical variability of the internal wave field: A search for sources and sinks, *J. Phys. Oceanogr.*, *6*, 471–485, 1976.

Wunsch, C., and S. Webb, The climatology of deep ocean internal waves, *J. Phys. Oceanogr.*, *9*, 235–243, 1979.

T. E. Ewart and S. A. Reynolds, Applied Physics Laboratory, University of Washington, Seattle, WA 98105.

J. D. Irish, University of New Hampshire, Durham, NH 03824.

M. D. Levine, College of Oceanography, Oregon State University, Corvallis, OR 97331.

(Received November 30, 1985;
accepted February 3, 1986.)